MIXED-MODE CRACK GROWTH IN TOUGHENED PMMA

L. ANDENA[1], A. CORIGLIANO[2], R. FRASSINE[1], S. MARIANI[2]
[1]Dipartimento di Chimica, Materiali e Ingegneria Chimica "Giulio Natta", Politecnico di Milano, Milano (ITALY)
[2]Dipartimento di Ingegneria Strutturale, Politecnico di Milano, Milano (ITALY)

ABSTRACT

Experimental results concerning mixed-mode crack growth in PMMA specimens are presented, together with numerical simulations of the whole fracture process. The mixed-mode tests were conducted on single edge notched specimens subject to three point bending loading conditions. The mode-mixity of the fracture loading was obtained by means of a notch offset with respect to the mid-span cross section. A generalized finite element approach was adopted for the numerical simulations, coupled with a local description of the fracture process based on a mixed-mode cohesive law.

1 INTRODUCTION

Mixed-mode fracture is an important issue in many engineering applications, and the number of the published research on the subject has been steadily growing in the most recent years [1, 2, 3, 4, 5]. In many practical situations, even components having relatively simple geometry and loading conditions (like films, composite plates and adhesive joints) may undergo mixed-mode fracture due to different combinations of service loadings and hygrothermal stresses. Under these conditions, crack initiation will be associated to different critical strain energy release rates at varying the mode-mixity ratio. As far as damage-tolerant design is concerned, the need for quantitative prediction of the remaining lifetime of a component also requires the crack propagation stage to be analysed. This may take place along a very complex crack path depending on material microstructure, loading conditions and component geometry, usually undergoing a transition from shear to opening fracture mode for most practical situations.
In the present paper, the mixed-mode fracture behaviour of a rubber-modified polymetyl methacrylate was characterised using asymmetric three point bending testing geometry. The fracture behaviour was simulated using a generalized finite element approach coupled with a local description of the fracture process using a specially formulated mixed-mode cohesive law, and the results were compared in order to get some insights about the transition from stable to unstable crack propagation.

2 MIXED-MODE THREE POINT BENDING TESTS ON PMMA

The material used in this study was a rubber toughened polymethyl methacrylate (PMMA) with 22 wt% of acrylic rubber, supplied in form of extruded sheets with nominal thickness $B = 8$ mm. The glassy matrix has weight and number average molecular weights of 134000 and 68000, respectively. The glass transition temperature of the matrix is 105 °C, while that of the rubbery phase is -30 °C.
A three point bending (TPB) test configuration was considered, using single edge notched specimens. The geometry of the specimens is shown in Fig. 1. The specimens has width W twice the thickness B and the span S is four times W.
Notching was performed in two stages. In the first one a notch was made with a 0.015 mm radius blade moving alternatively into the specimen. In the second one, the same blade was pushed into the previously prepared notch after cooling the material to -40 °C so as to propagate a short brittle crack: the blade works as a wedge and causes the formation of a natural crack ahead of the machined notch. The highly stressed zone that developed ahead of the notch tip during the machining operation was removed by annealing the specimens at 90 °C for 5 h and then cooling it to 23 °C at a rate of 1 °C/min [6]. Two different initial notch depths a_0 were considered, corresponding to a_0/W ratios of 0.3 and 0.6. In order to ensure mixed-mode crack loadings, the notches were performed at a varying distance d from the mid-span cross section of the specimens: three different offset ratios $\chi \equiv 2d/S$ of 0.25, 0.50 and 0.75 were used.
Fracture testing was conducted at 23 °C and at constant crosshead displacement rate $du/dt = 5$ mm/min with an Instron 1185 dynamometer. A 10 kN load cell was used to measure the load P.

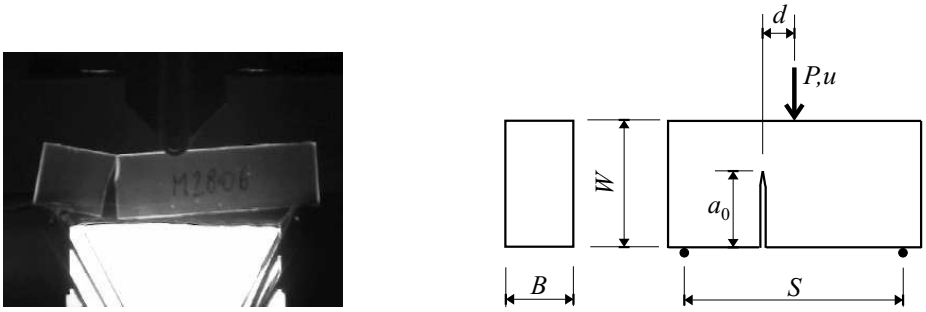

Figure 1: mixed-mode TPB test. Test set-up, geometry and notation.

3 NUMERICAL SIMULATIONS

The extended finite element method for quasi-brittle fracture proposed in [7, 8] was here adopted for the numerical simulation of the mixed-mode TPB tests discussed in Section 2.

Let us consider a two-dimensional body Ω with boundary $\Gamma = \Gamma_t \cup \Gamma_u$: tractions are prescribed on Γ_t and displacements on Γ_u. Let Γ_d be a propagating discontinuity locus inside Ω; along Γ_d a cohesive interaction between the two flanks exists in the process zone (PZ).

The equilibrium conditions for Ω are:

$$\boldsymbol{\mathcal{C}}^{\mathrm{T}}\boldsymbol{\sigma} + \bar{\boldsymbol{b}} = \boldsymbol{0} \qquad \text{in } \Omega\backslash\Gamma_d; \tag{1}$$

$$\boldsymbol{N}\boldsymbol{\sigma} = \bar{\boldsymbol{t}} \qquad \text{on } \Gamma_t; \tag{2}$$

$$\boldsymbol{M}\boldsymbol{\sigma} = -\boldsymbol{t}^+ \qquad \text{on } \Gamma_d^+ \,, \qquad \boldsymbol{M}\boldsymbol{\sigma} = \boldsymbol{t}^- \qquad \text{on } \Gamma_d^- . \tag{3}$$

Here: $\boldsymbol{\sigma}$ is the stress vector; $\bar{\boldsymbol{b}}$ and $\bar{\boldsymbol{t}}$ are the prescribed external loads per unit volume and surface, respectively; $\boldsymbol{\mathcal{C}}$ is the differential compatibility operator; $\boldsymbol{N}$ and $\boldsymbol{M}$ are matrices containing the components of the unit outward normal $\boldsymbol{n}$ to Γ and of the unit normal $\boldsymbol{m}$ to Γ_d. Γ_d^+ and Γ_d^- respectively define the two flanks of Γ_d acted upon by the traction vectors $\boldsymbol{t}^+$ and $\boldsymbol{t}^-$. The equilibrium across Γ_d thus reads:

$$\boldsymbol{t} \equiv \boldsymbol{t}^- = -\boldsymbol{t}^+ . \tag{4}$$

The linearized compatibility conditions in $\Omega\backslash\Gamma_d$ and along Γ_u are given by:

$$\boldsymbol{\varepsilon} = \boldsymbol{\mathcal{C}}\boldsymbol{u} \qquad \text{in } \Omega\backslash\Gamma_d; \tag{5}$$

$$\boldsymbol{u} = \bar{\boldsymbol{u}} \qquad \text{on } \Gamma_u, \tag{6}$$

$\boldsymbol{\varepsilon}$ and $\boldsymbol{u}$ being the strain and the displacement vectors, respectively, and $\bar{\boldsymbol{u}}$ the assigned displacements along Γ_u. The displacement discontinuity $[\boldsymbol{u}]$ across Γ_d can be expressed as:

$$[\boldsymbol{u}] = \boldsymbol{u}\Big|_{\Gamma_d^+} - \boldsymbol{u}\Big|_{\Gamma_d^-} . \tag{7}$$

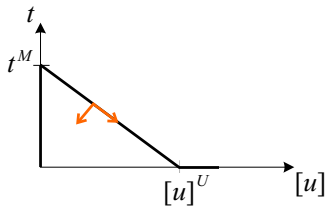

Figure 2: mixed-mode effective cohesive law.

As far as the constitutive law is concerned, the bulk material in $\Omega\backslash\Gamma_d$ is assumed to behave elastically, i.e.:

$$\boldsymbol{\sigma} = \boldsymbol{D}_\Omega \boldsymbol{\varepsilon} \qquad \text{in } \Omega\backslash\Gamma_d, \tag{8}$$

$\boldsymbol{D}_\Omega$ being the bulk stiffness matrix.

A cohesive model is adopted for the PZ. Following [9], an effective displacement discontinuity $[u]$ is defined according to:

$$[u] = \sqrt{[u]_n^2 + \beta^2 [u]_s^2}, \tag{9}$$

where: $[u]_n$ and $[u]_s$ are, respectively, the opening and sliding components of the displacement discontinuity vector $[\boldsymbol{u}]$; β^2 is a coupling coefficient that represents the ratio between mode II and mode I fracture energies [10, 11]. The effective cohesive law is then defined as in Fig. 2, with a linear softening envelope and an effective fracture energy $G_c = t^M [u]^U/2$. Loading/unloading conditions in the softening branch are formulated according to a damage law, such that unloading to the origin of the $t - [u]$ plane (see Fig. 2) is guaranteed (details can be found in [7]).

At fixed Γ_d, the weak form of the governing relations, account taken of the constitutive laws for the bulk material and for the cohesive PZ, reads:

$$\text{find } \boldsymbol{u} \in \mathcal{U} : \int_{\Omega\backslash\Gamma_d} \boldsymbol{\varepsilon}^{\mathrm{T}}(\boldsymbol{v})\, \boldsymbol{D}_\Omega \dot{\boldsymbol{\varepsilon}}(\dot{\boldsymbol{u}})\, d\Omega + \int_{\Gamma_d} [\boldsymbol{v}]^{\mathrm{T}} \boldsymbol{R}^{\mathrm{T}} \boldsymbol{D}_\Gamma \boldsymbol{R} [\dot{\boldsymbol{u}}]\, d\Gamma_d = \int_{\Omega\backslash\Gamma_d} \boldsymbol{v}^{\mathrm{T}} \dot{\bar{\boldsymbol{b}}}\, d\Omega + \int_{\Gamma_t} \boldsymbol{v}^{\mathrm{T}} \dot{\bar{\boldsymbol{t}}}\, d\Gamma_t \quad \forall \boldsymbol{v} \in \mathcal{U}_0, \tag{10}$$

where: a superposed dot stands for rates; $\mathcal{U}$ is the space of admissible displacements $\boldsymbol{u}$ in Ω, i.e. such that $\boldsymbol{u} = \bar{\boldsymbol{u}}$ on Γ_u, $\boldsymbol{u}$ possibly discontinuous on Γ_d; $\boldsymbol{v} \in \mathcal{U}_0$ (with zero prescribed displacements on Γ_u) is the test function; $\boldsymbol{D}_\Gamma$ is the cohesive tangent stiffness matrix; $\boldsymbol{R}$ is the orthogonal global-local mapping along Γ_d.

To simulate cohesive crack growth in the frame of the extended finite element method, the displacement field is assumed [7, 8]:

$$\boldsymbol{u}^h(\boldsymbol{x}) = \sum_{i \in I} \phi_i(\boldsymbol{x})\, \boldsymbol{u}_i^0 + \sum_{j \in J} \mathcal{H}(\boldsymbol{x})\, \phi_j(\boldsymbol{x})\, \boldsymbol{u}_j^E, \tag{11}$$

where: the set I collects all the nodes, whose overlapping supports completely cover Ω, while J gathers only those nodes whose supports are even partially cut by Γ_d; $\boldsymbol{u}_i^0$ are the customary nodal degrees of freedom and $\boldsymbol{u}_j^E$ are the additional ones; ϕ_i is the piece-wise linear nodal shape function; $\mathcal{H}(\boldsymbol{x})$ is the generalized Heaviside step-function:

$$\mathcal{H}(\boldsymbol{x}) = \begin{cases} +1 & \text{if } (\boldsymbol{x} - \boldsymbol{x}^*)^{\mathrm{T}} \boldsymbol{m} > 0 \\ -1 & \text{if } (\boldsymbol{x} - \boldsymbol{x}^*)^{\mathrm{T}} \boldsymbol{m} < 0 \end{cases} \tag{12}$$

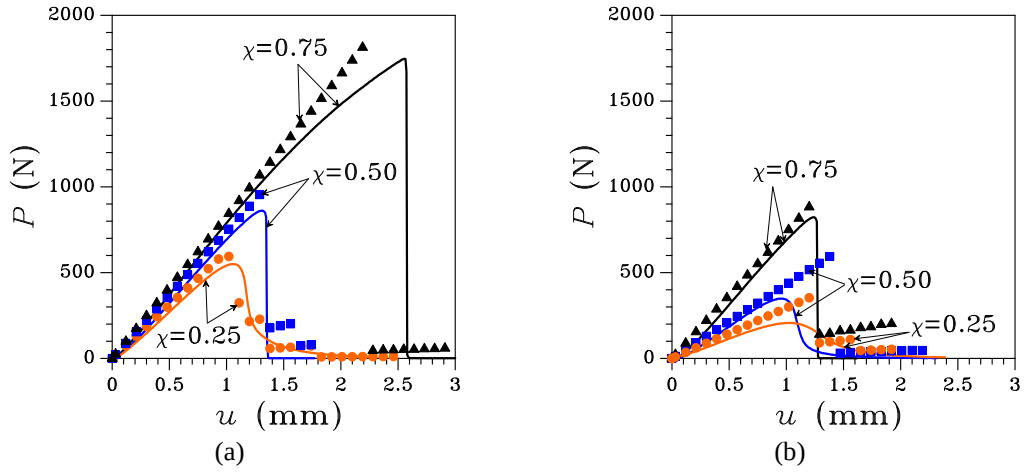

Figure 3: mixed-mode TPB test. Comparison between experimental (continuous lines) and numerical (filled symbols) load-displacement plots: (a) $a_0/W = 0.3$; (b) $a_0/W = 0.6$.

$\boldsymbol{x}^*$ being the closest point projection of the generic point $\boldsymbol{x} \in \Omega$ onto Γ_d (see also [8]). This discretization gives rise to a piece-wise linear continuous displacement field in $\Omega \backslash \Gamma_d$ and a piece-wise linear displacement discontinuity along Γ_d, provided that the Γ_d tip is always located at the edge of an element.
To propagate Γ_d, the stress state ahead of the current crack tip is recovered in a patch of elements whose integration points are located inside a circle centered at the Γ_d tip and with a radius of up to n_r times the characteristic mesh size (in the forthcoming examples $n_r = 8$ was used). A fourth-order complete polynomial function is best-fitted to the recovered stress field and, on its basis, crack growth direction is assumed perpendicular to the maximum in-plane principal stress σ_p at the crack tip. According to this criterion, the crack starts propagating as soon as σ_p exceeds the tensile strength t^M; at fixed loading conditions, the crack then grows until the condition $\sigma_p < t^M$ is satisfied.

4 RESULTS

To assess the capability of the proposed extended finite element method to simulate mixed-mode crack growth, results for the TPB tests of Section 2 are presented.
The PZ cohesive law was calibrated by matching the experimental and numerical load vs displacement plots in the case $a_0/W = 0.3$ and $\chi = 0.25$, obtaining: $t^M = 50$ MPa, $G_c = 2.5$ N/mm. The elastic properties of the bulk were assumed: Young's modulus $E = 1900$ MPa, Poisson's ratio $\nu = 0.39$. These parameter values guarantee a good agreement between experimental data and numerical outcomes, both in the hardening and in the softening regimes.
As for the load vs displacement relation, it emerges that only for $a_0/W = 0.6$ and $\chi = 0.50$ the numerical response is significantly more brittle than the experimental one, and characterized by the sudden drop of the plot at $u \cong 1.4$ mm. In all the other cases, the eventual steep softening branch is correctly captured and linked to a sudden, unstable propagation of the crack after an initial stable phase.
As far as the failure mode is concerned, in Figs. 4 and 5 the final crack paths are reported for $a_0/W = 0.3$ and 0.6, respectively. It can be seen that propagation of the crack within the elements allows to obtain results completely independent of the background mesh.
As already noted in [7], by increasing the offset ratio χ, for any a_0/W, the test is characterized by: an increased initial stiffness (slope of the $P - u$ curve) in the hardening regime; a transition from a whole

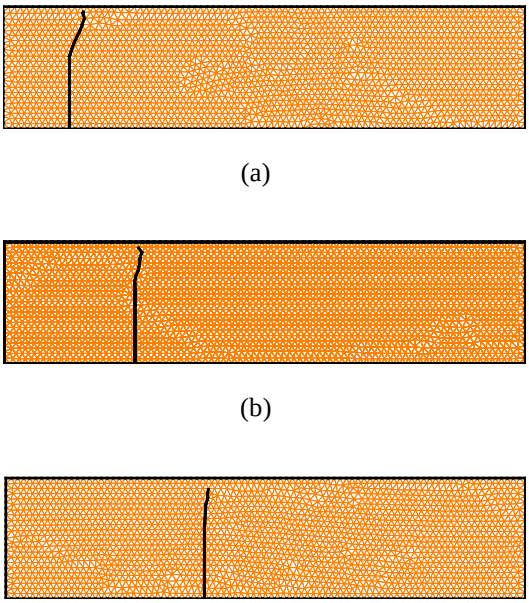

Figure 5: mixed-mode TPB test. Simulated crack paths for $a_0/W = 0.6$: (a) $\chi = 0.75$; (b) $\chi = 0.50$; (c) $\chi = 0.25$.

[5] K.S. Madhusudhana and R. Narasimhan. Experimental and numerical investigations on mixed-mode crack growth resistance of a ductile adhesive joint. *Engineering Fracture Mechanics*, 69:865–883, 2002.

[6] ISO 13586. *Plastics – Determination of fracture toughness (GIC and KIC) – Linear elastic fracture mechanics (LEFM) approach*. International Organization for Standardization, 2000.

[7] S. Mariani and U. Perego. Extended finite element method for quasi-brittle fracture. *International Journal for Numerical Methods in Engineering*, 58:103–126, 2003.

[8] C. Comi, S. Mariani, and U. Perego. From localized damage to discrete cohesive crack propagation in nonlocal continua. In H.A. Mang, F.G. Rammerstorfer, and J. Eberhardsteiner, editors, *Proceedings of the Fifth World Congress on Computational Mechanics (WCCM V)*. Vienna University of Technology, 2002.

[9] G.T. Camacho and M. Ortiz. Computational modelling of impact damage in brittle materials. *International Journal of Solids and Structures*, 33:2899–2938, 1996.

[10] M. Ortiz and A. Pandolfi. Finite-deformation irreversible cohesive elements for three-dimensional crack-propagation analysis. *International Journal for Numerical Methods in Engineering*, 44:1267–1282, 1999.

[11] A. Corigliano, S. Mariani, and A. Pandolfi. Numerical analysis of rate-dependent dynamic composite delamination. *Composites Science and Technology*, to appear, 2004.